Supplementary information

Supercritical fluid electrodeposition, structural and electrical characterisation of tellurium nanowires

Philip N. Bartlett[a], David A. Cook[a], Mahboba M. Hasan[a], Andrew L. Hector[a], Sam Marks[b], Jay Naik[c], Gillian Reid[a], Jeremy Sloan,[b] David C. Smith[c], Joe Spencer[c], Zondy Webber[c]

Table S1. Review of literature on tellurium nanowires.

Method of preparation is highlighted by colour: pink = electrochemical, green = solvothermal, yellow = PVD and white = other.

Publication	Growth method	Dimensions	Form/structure	Application/measurements	Reaction time/growth rate.
Electrochemical					
Ivanou *et al.*[1]	Electroplating into AAO from 1 mM TeO_2 in 0.1 M HNO_3.	60 nm Ø average.	Amorphous by XRD. 220 nm long. Wires not removed from template.	NA	~31 nm per minute.
Keilbach *et al.*[2]	Electrodeposition into hierarchical mesoporous silica-anodic alumina template. 1 mM TeO_2, 0.5 M K_2SO_4 in water.	Average of 10 nm Ø. TEM suggests ~5-15 nm Ø typical.	Micron length scale.	NA	Incomplete filling of template after >12 hr corresponding to < 80 nm/min.
Li *et al.*[3]	Template-free and surfactant-free electrochemical deposition	60-80 nm Ø rods (2-4.5 µm long).	Pure single crystalline hexagonal phase Te. Short bundles of rods bound at Ti surface. <001> growth direction.	Photoconductive properties. Conductivity of nanowire film increased under simulated sunlight (1.07 × i) or UV (1.05 x i).	15 min.

	method in 0.1 M Na_2TeO_3 aqueous solution.				
Xiang *et al.*[4]	Electrodeposition into individually addressable anodic alumina pores. 1 mM TeO_2 solution in 0.5 M K_2SO_4.	27 nm average Ø.	Wires confined in alumina template.	NA	Unclear .
Zhao *et al.*[5]	Electrodeposition into anodic alumina from TeO_2 in aqueous HCl solution.	60 nm Ø (40 µm long).	Confined hexagonal phase, single crystal wires with <001> growth direction.	The high optical polarization of the Te nanowire arrays embedded in the AAM assembly system was observed.	24 h.
She *et al.*[6]	Template-Free electrodepositio n onto indium doped tin oxide (ITO) from TeO_2 powder in 1 M KOH aqueous solution.	50 to 500 nm Ø (tens of microns long).	Single crystalline trigonal structure Te nanowires. <001> growth direction. Other structures such as ribbons and tubes also formed in same deposition.	NA	30 min.
Solvothermal					
Li *et al.*[7]	Solvothermal reduction of TeO_2 with NaOH in presence of polyvinyl pyrrolidone (PVP) in ethylene glycol.	72 nm Ø wires (3.8-4.2 µm long) 240 nm Ø tubes (4-6 µm long. Inner Ø=152 nm.	Single crystal, wires and tubes. Preferential growth <001>. Hexagonal cross-sections.	NA	~1 h.
Wang *et al.*[8]	One pot	7-9 nm Ø.	Several microns. Single	Used to make telluride wires	6 -10 hr to wires of

	hydrothermal. 1.36 M Na_2TeO_3 180 C in water.		crystal wires. <001> growth direction.	and carbonaceous nanofibers.	several microns (depending on reactor size).
Zhenghua *et al.*[9]	Hydrothermal recrystallization from Te powder in aqueous hydrazine hydrate solution.	Average 40 nm Ø Tubes (100-200 nm long with 40 nm wall thickness).	Several microns. Single crystalline, preferred <001> growth. Tubes are 1-2 microns long.	Gas sensing properties assessed.	6-12 h reaction time.
Liang and Qian[10]	Reduction of Na_2TeO_3 with $Na_2S_2O_3$ by hydrothermal reaction in presence of PVP.	10-40 nm Ø, average 27 nm.	Pure trigonal phase Te with growth along <001> planes. Single crystal wires, microns in length.	Single wire field effect transistor formed. Electrical properties characterized by two-electrode transport measurements.	>24 h.
Lu *et al.*[11]	Hydrothermal reduction of H_2TeO_4 with starch directing/reduc-ing agent.	25 nm average Ø.	Hexagonal phase. Single crystal. Up to 10 microns long. 001 growth direction.	NA	15 h.
Lu *et al.*[12]	Hydrothermal reduction of H_2TeO_4 with alginic acid directing/reduc-ing agent ("biomolecule assisted").	80 nm average Ø.	Hexagonal phase. Single crystal. Up to 10 microns long. <001> growth direction.	NA	15 h.
Cao *et al.*[13]	Hydrothermal synthesis. Reduction of Na_2TeO_3 with	60 to 80 nm Ø (several microns long).	Short irregular rods of pure, crystalline, trigonal Te.	NA	12 h.

	glucose, cetyltrimethylammonium bromide (CTAB) as a structure-directing agent.				
Yuan *et al.*[14]	Hydrothermal reduction of orthotelluric acid ($Te(OH)_6$) with hydrazine (N_2H_4).	60 to100 nm Ø (tens of microns long).	Nanorods and particles (depending on [orthotelluric acid] concentration). Nanorods quite monodisperse. Crystalline hexagonal Te. <001> growth direction.	NA	24 h.
Qin *et al.*[15]	Low T (50-180 ^{o}C) Hydrothermal reaction of Na_2TeO_3 with hydrazine.	100 to 700 nm Ø (<5 µm long).	Prismatic Nanotubes of crystalline hexagonal Te with <001> growth direction.	NA	12-48 h.
Wang *et al.*[16]	Poly(ethylene glycol) mediated hydrothermal dissolution/recrystallization of Te powder.	200-400 nm Ø (5-20 µm long).	Hexagonal cross section nanotubes (wall thickness of ~30 nm). Single crystal trigonal Te with <001> growth direction.	NA	48 h.
Yan *et al.*[17]	Hydrothermal reaction of Na_2TeO_3 with hydrazine in presence of ammonium hydroxide and polyvinylpyrrolidone.	Average 30 nm Ø (~100 µm long).	Quite polydisperse wires. Single crystalline hexagonal phase. <001> growth direction.	Photocatalytic properties. Demonstrated photocatalytic decomposition of organic toluidine blue dye. 60% decomposition in less than 20 min (and 100 % in 60 min) in presence of Te nanowires.	3 h.

Liu *et al.*[18]	Hydrothermal reduction of Na_2TeO_3 by hydrazine in a mixed solution of ethanol and water in presence of poly(vinyl pyrrolidone) surfactant.	~25 nm Ø (tens of microns long) Also produced hexagonal tubes of micrometre diameter.	Single crystalline, trigonal Te with <001> growth direction.	NA	12-48 h.
Xi *et al.*[19]	Solvothermal reaction of TeO_2 in presence of poly(vinyl-pyrrolidone)	Nanowires of 23 nm Ø (16 hr synthesis) 10-20 nm Ø (55 hr synthesis) And nanotubes	Uniform, single crystal, trigonal Te wires of >10 microns length. <001> growth direction. Nanotubes also produced at intermediate times.	NA	16 -45 h.
Lin-Bao *et al.*[20]	Hydrothermal. sodium telluride (Na_2TeO_3) heated in the presence of sodium thiosulfate.	20–50 nm Ø (several microns long).	Single crystal, trigonal Te with <001> growth direction.	Electrical properties of individual TeNW-based field effect transistor measured and adjusted by doping. MoO_3 and Copper(II) phthalocyanine (CuPc) thin layer coating found to greatly enhance both electrical conductivities and hole concentrations.	20 h.
Panahi-Kalamuei *et al.*[21]	Solvothermal synthesis. Reduction of	H_2O solvent yields Diameters of	Short nanorods. hexagonal phase Te.	Photovoltaic measurements. Solar cell fabricated with paste of Te nanorods on	< 1h.

	$TeCl_4$ with hydrazine hydrate ($N_2H_4.H_2O$) in the presence of thioglycolic acid (TGA), cetyltrimethyl-ammonium-bromide (CTAB) and sodium dodecyl sulfate (SDS) surfactants.	30–40 nm (lengths of 200–300 nm). Methanol solvent yields diameters of 50–80 nm (lengths of 1–2 µm).		fluorine doped tin oxide substrate (FTO). J–V measurements indicated that the efficiency of the solar cell based on the Te nanorods was about 0.1%.	
Zhang *et al.*[22]	Solvothermal process. Te powder reacted with hydrazine and ammonia in range of solvents: acetone, methanol, isopropanol, tetrahydrofuran, ethylenediamine, ethanol, ethylene glycol and water.	100 nm Ø tubes with 15 nm walls. Nanorods of 50 nm Ø (200-400 nm long). Nanowires of 100-300 nm Ø (tens of microns long).	Single crystalline, hexagonal Te. Tubes, rods and wires formed depending on the solvent used and reaction time.	NA	2-20 h.
Thirumurugan [23]	Solvothermal synthesis from Te powder in imidazolium [BMIM]-based ionic liquids with	75 nm average Ø (tens of microns long).	Polydisperse wire mixtures (wide range of diameters and lengths). Hexagonal phase Te with <001> growth direction.	NA	10 h.

	polyethylene-glycol co-solvents.				
Physical Vapour Deposition					
Safdar *et al.*[24]	1 step PVD method. Catalyst free. Te powder heated to 700-800 C in Ar and H_2.	Tip diameter 15- 40 nm Ø.	Hexagonal Micro-columns with narrower tips (arrays). <001> growth, hexagonal single crystal.	Field emission measurements. Local field enhancement factor measured.	60-70 min.
Wang *et al.*[25]	1 step PVD from Te powder at 450–650 °C.	160 nm Ø.	Single crystal. 001 growth direction. Microscale triangle array, microscale hexagon array, microscale needle array and random-oriented nanoscale needle nanowires networks formed. <10 microns long.	Controlled wettability. Static and advancing/receding contact angles were measured.	30 min.
Hyung *et al.*[26]	Thermal evaporation of Te powder. PVD onto silicon wafer.	300-500 nm Ø rods (< 3 µm long) 200 nm Ø tubes (~10 µm long).	Microrods to nanorods and tubular nanostructures with Increasing T. Rods grown at an angle from compact 2D microcrystalline layer of Te. Triangular tubes. Single crystalline hexagonal Te with <001> growth direction.	NA	>2 h.
Sen *et al.*[27]	PVD onto alumina and	Te whiskers 150-200 nm Ø	Short whiskers grown on Te particles. Also large	NA	2 h.

	Si(111) substrates from Te powder source.	base to 50-70 nm Ø tips (tens of microns long). Te nanotubes of 150-500 nm Ø (2 µm average length).	150-500 nm diameter tubes formed on alumina and silicon substrates. Composed of hexagonal phase Te with <001> growth direction.		
Other					
Buhro *et al.*[28]	Decomposition of $TeCl_4$ in presence of trioctylphosphine oxide(TOPO) in polydecene soliton at 250-300 C.	30-60 nm Ø wires. mean Ø=41.8 nm.	Single crystal, micrometre scale length. <001> growth	NA	<3 min.
Xi *et al.*[29]	Surfactant assisted solid-solution-solid growth. Na_2TeO_3 reduced with ascorbic acid at low T (90 C). CTAB structure directing agent.	Average 7 nm Ø. 4-10 nm Ø range.	Single crystal. Tens of microns long. Uniform. 001 growth direction.	Luminescence measured.	20 h reaction time.
Liu *et al.*[30]	Te nanowire arrays from LB technique. Synthesis described	7 nm Ø		Made telluride wires and heterojunctions of Te with tellurides. Measured photoconductive and electrical properties.	?

	elsewhere.				
Liu *et al.*[31]	Reduction of $[TeS_4]^{2-}$ with SO_3^{2-} in presence of sodium dodecyl benzenesulfonate. Surfactant assisted, solid-solution-solid growth.	14 nm Ø	300 nm long. Single crystal, hexagonal phase of Te. Consistent lengths, uniform rods with <001> growth direction.	NA.	12-24 h. Growth rate of ~1.7 nm min^{-1}.
Jeong *et al.*[32]	Galvanic displacement of Si in 4.5 M HF bath containing 1 mM TeO_2 and 1 M $CdCl_2$ at room T.	87 nm average Ø.	Disordered conical, single-crystal, hexagonal, columns of ~2.3 µm long. <001> growth direction.	Piezoelectric properties measured. Maximum output current of -75 nA.	96 h.
Mo *et al.*[33]	Disproportion-ation of sodium tellurite (Na_2TeO_3) in aqueous ammonia at 180 ^oC.	Nanobelts 8 nm average x 30-500 nm. Nanotubes 150-400 nm Ø, wall thickness 5-15 nm.	Single crystal nanobelts (hundreds of microns long by 5-20 nm thick) and nanotubes (5-10 microns long. Helical nanobelts probably grow into the tubes as they get wider. <001> growth direction.	NA	36 h.
Wang *et al.*[34]	ZnO nanorod templating-reaction. ZnO–CdTe nanocable arrays-on-ITO soaked in ammonia solution, leading	150 nm Ø nanotubes (wall thickness 60 nm, 8 µm long). Rods of 17 nm Ø (~80 nm long).	Vertically aligned nanotubes and nanorods branched from CdTe nanotubes. Nano-crystalline hexagonal Te. Nanostructures are confined but not highly ordered.	NA	1 h.

	to etching of ZnO core and partial reduction of the CdTe shell.				
Lilly *et al.*[35]	Slow oxidation of unstabilised CdTe nanoparticles in aqueous DMSO solution	Average 130 nm Ø (6 to 15 µm long)	Tortuous wires. <001> growth direction. Contain traces of the seed elements. Incorporation of Se into wire increases tortuosity.	NA	1-3 days.
Webber *et al.*[36]	Photolysis of tBu_2Te_2 in an aqueous micellar system incorporating dodecanethiol as an auxiliary morphology-directing agent.	Average 12.7 ± 3.0 nm Ø (average length 46.5 ± 9.4 nm).	Short rods of pure single crystal trigonal Te. <001> growth direction.	NA	12 h.
Toshima and Watanabe[37]	Reduction of Tellurium(IV) ethoxide with sodium borohydride with poly(N-vinyl-2-pyrrolidone) (PVP) or trioctylphosphine oxide (TOPO) as protecting agents.	Average 10 nm Ø (average length of 30 nm).	Short rods of hexagonal phase Te.	NA	>8 h.
Gautam *et al.*[38]	Solvation and recrystallization	15–30 nm Ø (~200 nm	Crystalline hexagonal Te rods.	Scanning tunnelling spectroscopy used to	?

	of Te nanoparticles formed *in situ* by spontaneous disproportionation of Sodium hydrogen telluride.	long)		investigate electron transport properties of Te nanorods. Band gap ~0.4 eV close to bulk Te value. Conductance increased with rod diameter.	
Haakenaasen *et al.*[39]	Gold seeded Molecular beam epitaxy onto silicon.	15-75 nm Ø.	Segmented single crystalline wires of hexagonal <001> Te with cubic <111> HgTe. Up to 1.5 µm long.	NA	?
Cheng *et al.*[40]	Self-extrusion from Si–Sb–Te thin films.	10-30 nm Ø (hundreds of microns long).	Individual, single-crystalline Te nanowires rooted to the substrate. <001> growth direction.	NA	1 nm s^{-1} under electron beam illumination, or weeks of photo illumination.
Kim and Park[41]	Reduction of sodium tellurite (Na_2TeO_3) by ethylene glycol solvent in presence of polyvinyl-pyrrolidone (PVP) and sodium thiosulfate ($Na_2S_2O_3$) surfactants.	Nanotubes 150-250 nm Ø (5-8 µm long and wall thicknesses of 70-80 nm).	Structurally uniform single crystal, hexagonal, prismatic, tubes. Hexagonal phase Te. <001> growth direction.	NA	1 h.
Zheng *et al.*[42]	spontaneous oxidation of NaHTe at room	15-30 nm average Ø (hundreds of	The nanorods display a tapered, triangular cross-section. Single	NA	24 h.

	temperature, in presence of sodium dodecyl benzene-sulfonate.	nm long).	crystal, hexagonal Te with 001 growth direction.		
Zhu *et al.*[43]	Ultrasound induced growth from tellurium nitrate solution in aqueous NaOH with polyethylene glycol and D-glucose.	30–60 nm Ø (200-300 nm long).	Single crystalline rods with irregular walls but uniform diameters. <001> growth direction.	NA	>24 h.

Device Fabrication Protocols

Standard Substrates. 1 cm squares of 100 nm thick silicon oxide coated N<100>P silicon wafers with resistivity 1-10 Ωcm^{-1} (IDB technologies ltd.) were used as substrates for the preparation of the tellurium transistors. These were prepared with an aluminium ohmic back contact with sub 10 Ω contact resistance, predefined Cr/Au bond pads, and a grid of fiducial markers on top of the oxide allowing the position of nanowires to be determined to better than 50 nm over an approximately 90×90 micron square field and large area bond Cr/Au bond pads (see Figs. S1 and S2 for the designs). e-beam pattern files used for defining the bond pads and fiducial markers are available from the authors.

Freed nanowires were drop cast onto these substrates. Four independent electrodes were then patterned onto the nanowires either by e-beam lithography and lift-off, allowing contacts to be made with 200 nm Ni or 5 nm Cr/ 200 nm Au, or using direct deposition of W via electron beam induced deposition (10-15 nm) followed by ion beam induced deposition of W and C (100 nm) both from tungsten hexacarbonyl.

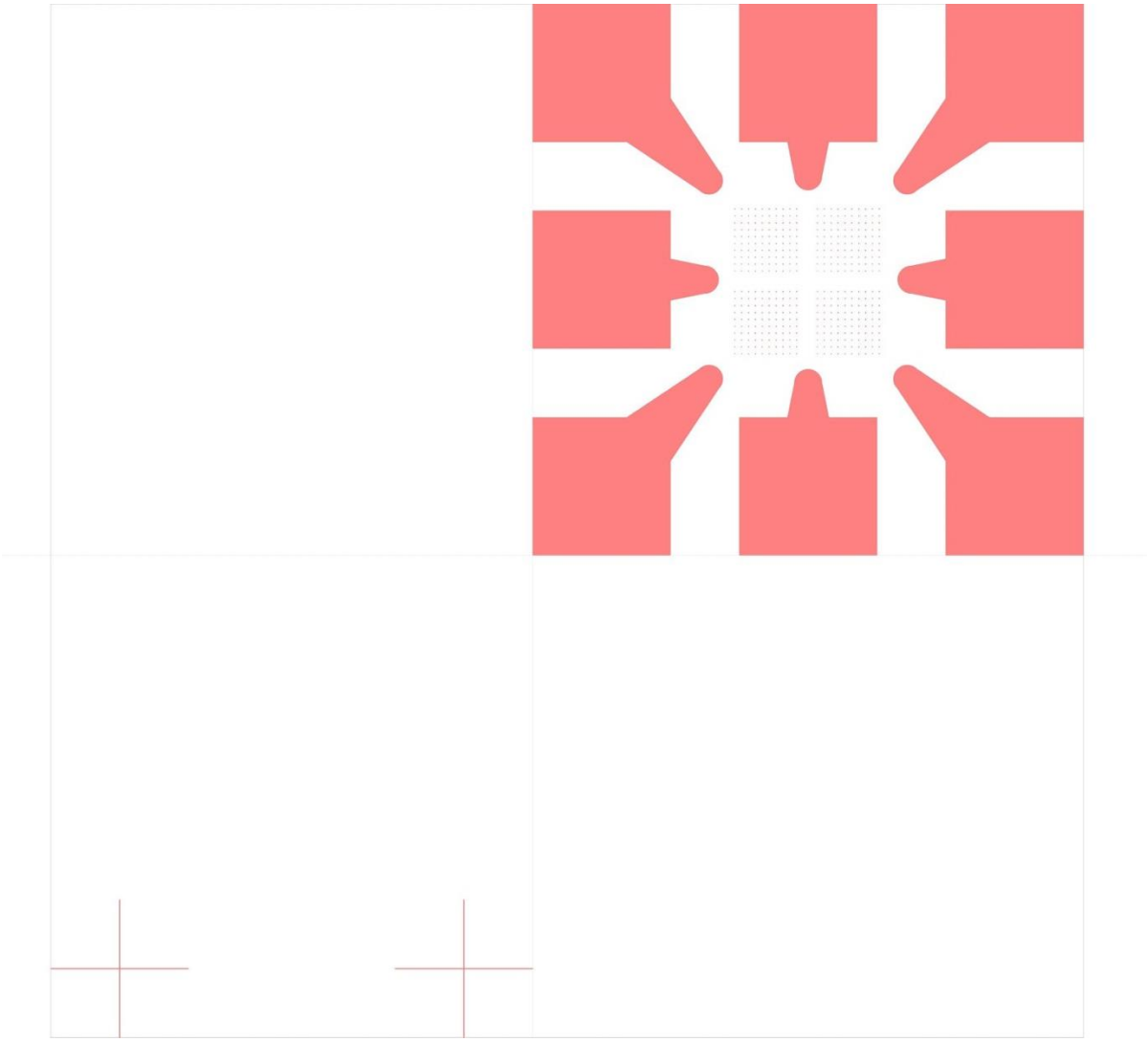

Fig. S1 Image showing metal structure predefined on top of substrates used for transistor production. The bottom left crosses are used for course alignment relative to the eight bond pads and four fine fiducial marker grids.

Fig. S2 Zoomed in image of fiducial marker grids. Each grid position is different allowing its position within the grid to be determined from an SEM image.

EBID/FBID Method. The electron beam-induced deposition (EBID) / focused ion beam induced deposition (FBID) prepared transistor samples were produced using a Zeiss NVision40 dual column system; a liquid Ga focused ion beam and a field emission gun scanning electron microscope (FEGSEM). The FEGSEM was used to image the tellurium nanowires which had been previously drop cast onto the standard oxide coated silicon substrates. The individual nanowires to be contacted were chosen from the images ensuring that they were sufficiently isolated from other nanowires, of a reasonable length and not

obviously forked or otherwise unusual. Tungsten hexacarbonyl was then introduced into the vacuum chamber and e-beam induced deposition, following the instrument manufacturer's standard procedure, used to deposit the parts of the contact directly on the nanowire. A layer of approximately 10-15 nm of tungsten was deposited in this step. The e-beam process is relatively slow compared with focused ion beam deposition but leads to purer tungsten and the deposit helps to protect the nanowire from ion beam damage in the FBID deposition. Next, focused ion beam deposition was used, following the the instrument manufacturer's standard procedure, to lay down a thicker layer of tungsten onto the EBID deposited parts of the contacts and to connect these parts to the bond pads previously defined on the substrate. The samples were imaged after deposition to check the contacts had been correctly deposited.

E-beam lithography method. To prepare the contacts using e-beam lithography standard substrates with tellurium nanowires drop coated onto it were first imaged using a Jeol JSM 7500F FESEM to determine the position of suitable tellurium nanowires, i.e. of sufficient length, not forked or otherwise unusual, and sufficiently isolated from their neighbours, and any large deposits of nanowires which might interfere with the contacting. These images were then used to determine the position of target nanowires and any objects to be avoided relative to the fiducial markers (Fig. S2). These objects were then entered into the e-beam pattern file on an otherwise unused pattern layer to aid the design of the contacts. A pattern for the contacts was then designed in a separate layer to connect the nanowire to the bond pads on the standard substrates. The contacts were separated into two components; a 200 nm wide section near the nanowire and a separate 1 micron wide section which connected the finer contacts to the bond pads. The substrates were then

prepared with a nominally 350 nm layer of poly(methyl methacrylate) (PMMA) resist (495PMMA A6, Microchem) by spin coating. The e-beam patterning was performed using a Leo 1455VP SEM fitted with a Raith Elphy e-beam lithography system. The patterning process involved a gross alignment stage using crosses remote from the bond pads shown in Fig S1. This stage allows positioning of the centre of the e-beam field to the centre of the bond pad and grid structure. The larger scale contact wires were then exposed into the resist. Next, a fine alignment step was performed for the grid containing a specific nanowire using fiducial markers chosen before the lithography run so that the inevitable exposure of the resist around these marks did not interfere with the patterned contacts. The fine structure of the contact pattern including the actual contacts to the nanowire was then written into the resist. After exposure the pattern was developed using methyl isobutyl ketone (MIBK):IPA 1:1 following the resist manufacturers standard procedure and inspected optically using a standard optical microscope. The metal for the contacts was then deposited using an e-beam evaporator and lift-off performed using acetone (Fisher HPLC grade). After patterning all samples were observed in a FEGSEM to determine the continuity of the contacts and ensure no metallic shorts remained. Based upon these images we were able to position the contacts with an accuracy of better than 50 nm onto the tellurium nanowires.

Electrical Characterisation.

Whilst the electrode design was bespoke for each nanowire, in general the width of each electrode on the wire was 200 nm and the minimum separation between the contacts 500 nm. A schematic representation of the device geometry is shown in Fig. S3 to enable the reader to better understand the electrical characterisation results.

The electrical characterisation of the nanowire transistor devices was performed using a Cascade M150 probe station and a MSA-400 Micro System Analyser with the device in the dark and at room temperature. Each sample was characterised to determine the pairwise resistances between all of the electrodes and the leakage behaviour between the electrodes and the silicon back gate. Any devices with significant defects were then discarded. Finally the gate dependent four point resistance of each nanowire was measured as a function of gate voltage. For some samples the combination of high channel resistance and bond pad capacitance meant that charging times were long, i.e. of the order of seconds, and so care was taken to ensure that the measurement time was sufficiently long that it had no effect on the final results.

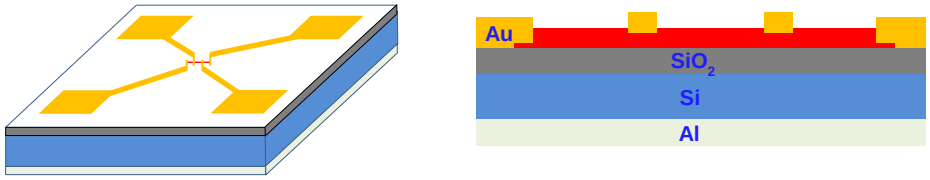

Fig. S3: Schematic of a complete nanowire transistor ready for 4 point measurement.

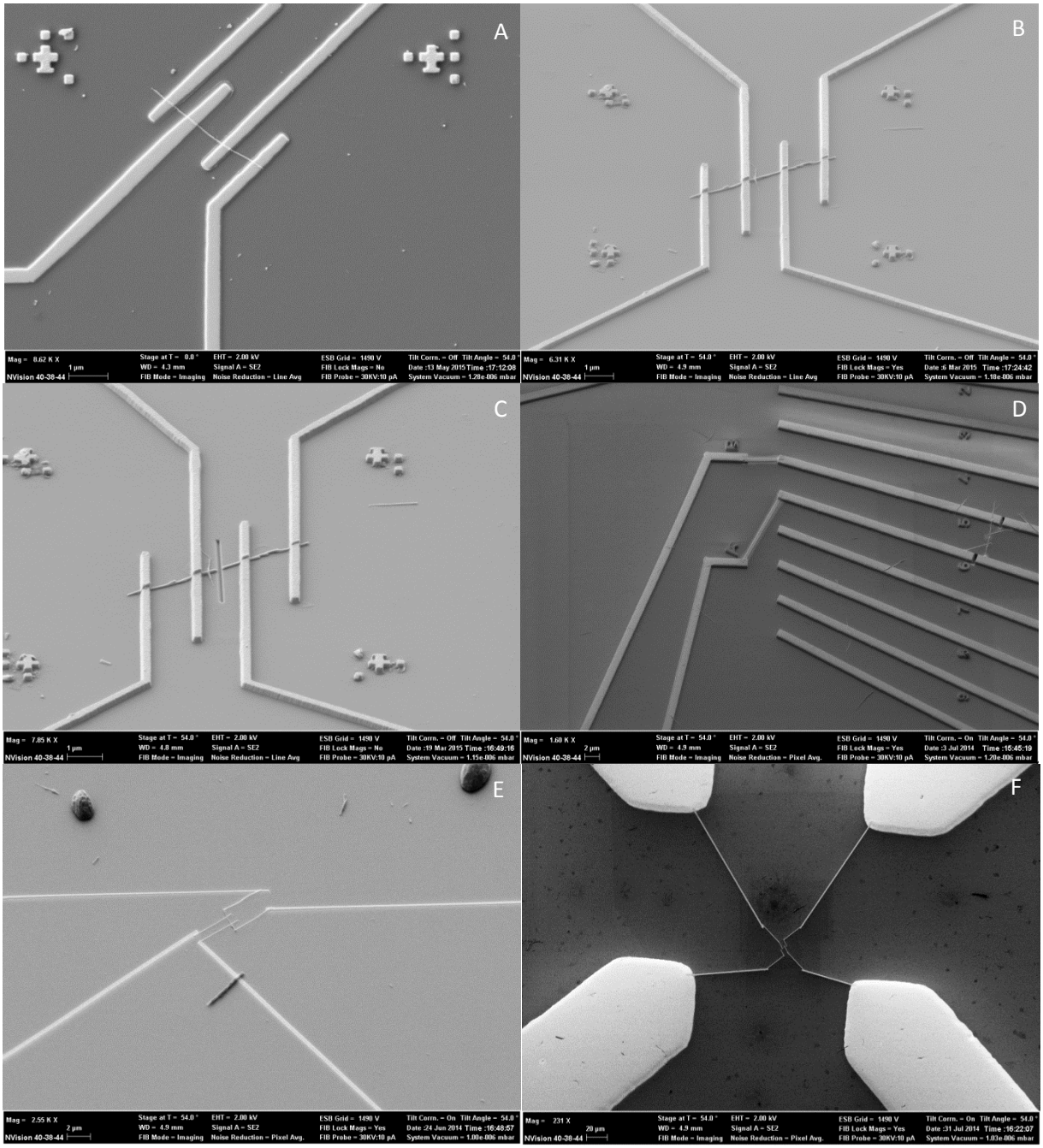

Fig. S4 EBL and FIB prepared samples for 4-point measurement A) 13 nm Te nanowire contacted using EBL with Ni, B) 55 nm Te nanowire contacted using EBL with Cr/Au, C) 55 nm etched using FIB to conduct 2 pt measurement, D) FIB-EBL combine process to fabricate multiple nanowire devices, E) FIB fabricated contacts to connect nanowire to the bond terminal arm, F) Successfully completed FIB fabricated 4-pt nanowire transistor.

Electrical Control Measurements. A number of control measurements were performed to support the electrical measurements. In particular substrates without tellurium nanowires

were patterned to determine the electrical resistance of a standard contact network by using the deposition system to define a 200 nm wide, 200 nm thick metal nanowire which was contacted using a standard pattern. The two point resistances measured between contacts on these substrates were considerably less than 1 KΩ. In addition, as shown in Fig. S4C a focused iIon beam was used to cut the tellurium nanowire in two successful transistors leading to no measurable current flow (<1 pA) between the contacts on either side of the cut.

Transistor measurements on TeNWs.

Thirty two nanowire transistor devices were prepared using 13, 35 and 55 nm nominal diameter nanowires from a variety of different deposition batches. Of these 13 were found to have significant defects, such as failed contacts or shorts to the gate. The 19 working devices covered a range of nanowire diameters and contact metals, Table S2.

Table S2 Summary of working Te nanowire transistors studied

Number of devices	Nominal Te NW diameter / nm	Contact type
2	13	Ni
2	55	Ni
3	13	Cr/Au
3	55	Cr/Au
1	13	W
2	35	W
5	55	W

Electrical measurements were performed with using a four point configuration. Each of the four electrodes plus the gate electrode was connected to a separate source measure unit (SMU) within the parameter analyser. One of the outer electrodes was designated as the ground connection. The SMU connected to the other outer electrode was set to voltage

source mode and designated as the first variable voltage. The SMUs connected to the two inner electrodes were set to current source mode with a zero input current and used to measure the potential between the two electrodes. The gate connection was connected to a high voltage SMU in voltage source mode and designated the second variable voltage. The effect of setting zero input current is that these connections to the sample become very high input impedance (> 1 TΩ) and thus the current flowing onto and off of the bond pads associated with these connections has to come via the nanowire which can lead to significant charging time. This was mitigated by scanning all voltages slowly and allowing sufficient settling times. To determine the gate dependent conductance of the nanowire the gate voltage was first set and the system allowed to settle for at least 10 s. The first variable voltage was then ramped from zero to 2 V and back to zero with a 1 mV step size and at least 1 s per step. Due to capacitive charging effects the current measured at the grounded electrode sometimes showed hysteretic behaviour. If this hysteresis was too great the experiments were performed more slowly until the hysteretic behaviour was only important over less than 10% of the scan. The conductance was determined by linear fits to plots of current versus the potential difference between the two intermediate electrodes for both the increasing voltage and decreasing voltage parts of each scan.

The gate dependence of the four point resistance of the transistors was measured for all 19 devices. In general, these were often noisy with the best results obtained on low resistance devices. The results from three of the low resistance devices are shown in Fig. S5. In each case there is small enhancement of the conductance of the device for negative gate potentials in line with what is expected from previous tellurium transistor measurements which tend to act as p-type transistors. However, the on-off ratios for the devices are much

smaller than for some of the previously published results for hydrothermally prepared TeNWs.[10, 20]

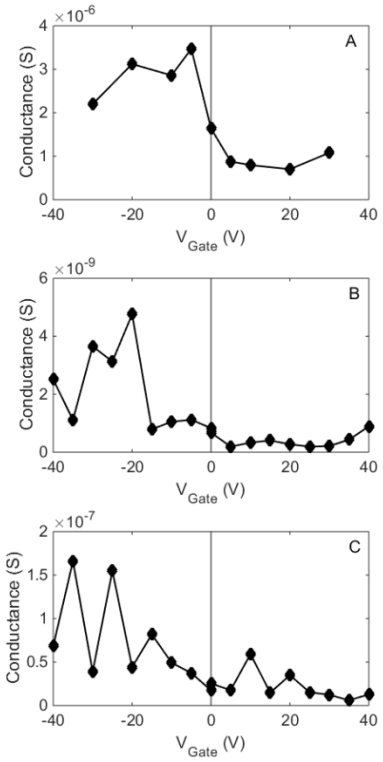

Fig. S5 Conductance of Te nanowire transistor channel versus gate voltage measured using four point technique for three of the higher conductance samples; A) 55 nm diameter nanowire with evaporated Cr/Au contacts, B) and C) two 13 nm diameter nanowires with evaporated Ni contacts.

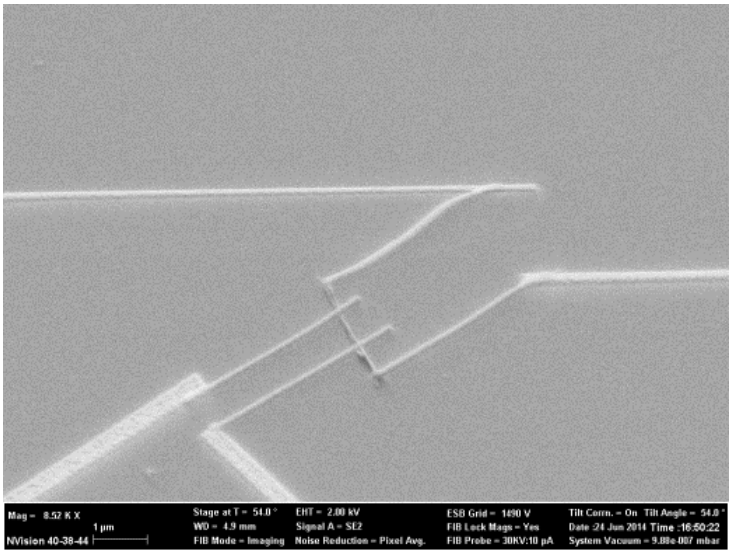

Fig. S6 SEM image of FIB contacted nanowire transistor

In particular, Luo et al.[20] have produced single TeNW transistors with diameters in the range 20-50 nm and channel length 2 μm with minimum resistance of 1.2 MΩ, an on-off ratio of ~100. It is difficult to explain the differences between the transistors presented here and in the work of Luo et al. We know from the XRD, Raman and TEM measurements that the SCFED deposited nanowires are crystalline Te. The fabrication processes used to produce the transistors presented here are not fundamentally dissimilar to those used by Luo et al. and the Raman spectra obtained from the channel of transistor devices shows the presence of tellurium and no other features.

Raman measurements on TeNWs.

Figs. S7 to 9 show additional Raman spectra of individual Te nanowires.

In Fig. S7 Spectra were taken with different grating configurations (900/900/1500 lines mm^{-1}) to improve SNR. This comes at a cost of the spectral resolution. No Te peaks were observed in the contacted wire. In the isolated NW, two clear modes for the A_1 and 2nd $E_{TO/LO}$ phonon are observed and their centre shift was determined by fitting to be 122.4 and 141.8 cm^{-1} respectively. The 1st $E_{TO/LO}$ phonon is slightly observable at the edge of the spectral window, fitting this peak determined a centre shift to be 94.3 cm^{-1}. Fig. S8 shows the Raman spectrum for an isolated Te NW. Fig. S9 shows repeat spectra collected on a single isolated TeNW. The peaks were fitted and centre shifts determined to be 100, 131 and 146.5 cm^{-1} for the first (blue spectrum) and 100.6, 128 and 145 cm^{-1} for second (orange spectrum). The positions of the bands are summarised in Table S3.

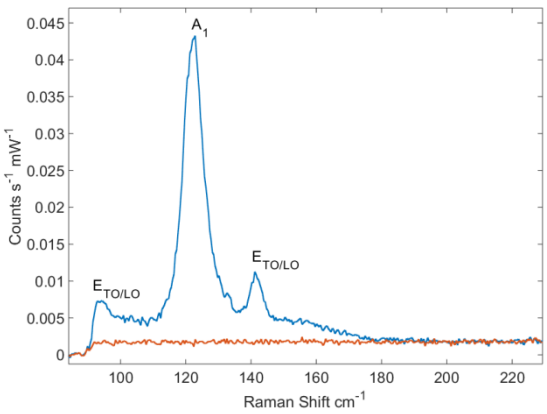

Fig. S7 Raman spectra on an isolated (blue) and contacted (orange) Te NW.

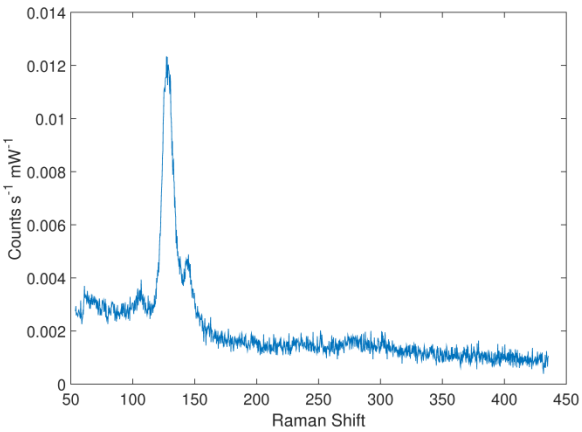

Fig. S8 Raman spectra of isolated Te NW. The spectrum shows 3 peaks at 103, 128 and 144cm^{-1}.

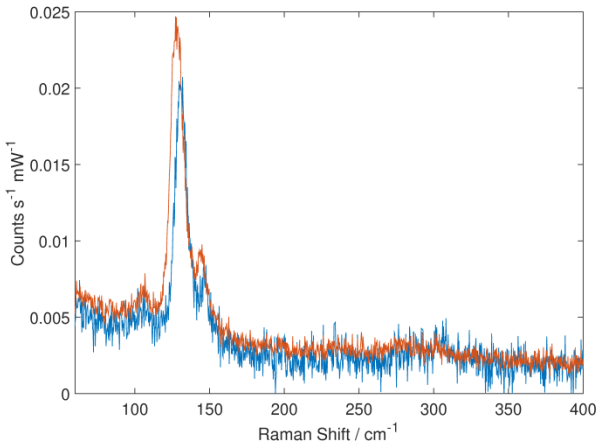

Fig. S9 Repeat spectra collected on same isolated NW sample

Table S3 Mean fitted Raman shifts for all available samples both contacted and non-contacted, along with the standard deviation.

Peak	Mean Shift (based on all spectra)	Standard Deviation
1st $E_{TO/LO}$	97.84 cm^{-1}	2.98 cm^{-1}
A_1	126.20 cm^{-1}	3.58 cm^{-1}
2nd $E_{TO/LO}$	144.65 cm^{-1}	2.08 cm^{-1}

References

1. D. K. Ivanou, Y. A. Ivanova, A. D. Lisenkov, M. L. Zheludkevich and E. A. Streltsov, *Electrochim. Acta*, 2012, **77**, 65-70.
2. A. Keilbach, J. Moses, R. Koehn, M. Doeblinger and T. Bein, *Chem. Mater.*, 2010, **22**, 5430-5436.
3. H. H. Li, P. Zhang, C. L. Liang, J. Yang, M. Zhou, X. H. Lu and G. A. Hope, *Cryst. Res.Technol.*, 2012, **47**, 1069-1074.
4. Y. Xiang, A. Keilbach, L. M. Codinachs, K. Nielsch, G. Abstreiter, A. Fontcuberta i Morral and T. Bein, *Nano Lett.*, 2010, **10**, 1341-1346.
5. A. Zhao, L. Zhang, Y. Pang and C. Ye, *Appl. Phys. A-Mater.*, 2005, **80**, 1725-1728.
6. G. She, W. Shi, X. Zhang, T. Wong, Y. Cai and N. Wang, *Cryst. Growth Des.*, 2009, **9**, 663-666.
7. Z. Li, S. Zheng, Y. Zhang, R. Teng, T. Huang, C. Chen and G. Lu, *J. Mater. Chem. A*, 2013, **1**, 15046-15052.
8. K. Wang, Y. Yang, H.-W. Liang, J.-W. Liu and S.-H. Yu, *Mater. Horiz.*, 2014, **1**, 338-343.
9. W. Zhenghua, W. Lingling, H. Jiarui, W. Hui, P. Ling and W. Xianwen, *J. Mater. Chem.*, 2010, **20**, 2457-2463.
10. F. Liang and H. Qian, *Mater. Chem. Phys.*, 2009, **113**, 523-526.
11. Q. Y. Lu, F. Gao and S. Komarneni, *Langmuir*, 2005, **21**, 6002-6005.
12. Q. Y. Lu, F. Gao and S. Komarneni, *Adv. Mater.*, 2004, **16**, 1629-+.
13. G. S. Cao, X. J. Zhang, L. Su and Y. Y. Ruan, *J. Exp. Nanosci.*, 2011, **6**, 121-126.
14. Q. L. Yuan, H. Y. Yin and Q. L. Nie, *J. Exp. Nanosci.*, 2013, **8**, 931-936.
15. A. M. Qin, Y. P. Fang and C. Y. Su, *Inorg. Chem. Commun.*, 2004, **7**, 1014-1016.
16. Z. Wang, L. Wang and H. Wang, *Cryst. Growth Des.*, 2008, **8**, 4415-4419.
17. C. Yan, C. M. Raghavan and D. J. Kang, *Mater. Lett.*, 2014, **116**, 341-344.
18. Z. P. Liu, S. Li, Y. Yang, Z. K. Hu, S. Peng, J. B. Liang and Y. T. Qian, *N. J. Chem.*, 2003, **27**, 1748-1752.
19. B. Xi, S. Xiong, H. Fan, X. Wang and Y. Qian, *Cryst. Growth Des.*, 2007, **7**, 1185-1191.
20. L.-B. Luo, F.-X. Liang, X.-L. Huang, T.-X. Yan, J.-G. Hu, Y.-Q. Yu, C.-Y. Wu, L. Wang, Z.-F. Zhu, Q. Li and J.-A. Jie, *J. Nanopart. Res.*, 2012, **14**, 967.
21. M. Panahi-Kalamuei, F. Mohandes, M. Mousavi-Kamazani, M. Salavati-Niasari, Z. Fereshteh and M. Fathi, *Mater. Sci. Semicond. Process.*, 2014, **27**, 1028-1035.
22. H. Zhang, D. R. Yang, X. Y. Ma and D. L. Que, *J. Cryst. Growth*, 2006, **289**, 568-573.
23. A. Thirumurugan, *Bull. Mater. Sci.*, 2007, **30**, 179-182.
24. M. Safdar, X. Zhan, M. Niu, M. Mirza, Q. Zhao, Z. Wang, J. Zhang, L. Sun and J. He, *Nanotechnol.*, 2013, **24**, 185705.
25. Q. Wang, M. Safdar, X. Zhan and J. He, *CrystEngComm.*, 2013, **15**, 8475-8482.
26. J.-H. Hyung, G.-S. Kim, A. K. Rai, C.-O. Jang, C.-Y. Lee, Z. Khurelbaatar, S. K. Acharya and S.-K. Lee, *J. Korean Phys. Soc.*, 2012, **60**, 47-50.

27. S. Sen, U. M. Bhatta, V. Kumar, K. P. Muthe, S. Bhattacharya, S. K. Gupta and J. V. Yakhmi, *Cryst. Growth Des.*, 2008, **8**, 238-242.
28. H. Yu, P. C. Gibbons and W. E. Buhro, *J. Mater. Chem.*, 2004, **14**, 595-602.
29. G. Xi, Y. Liu, X. Wang, X. Liu, Y. Peng and Y. Qian, *Cryst. Growth Des.*, 2006, **6**, 2567-2570.
30. J.-W. Liu, J. Xu, H.-W. Liang, K. Wang and S.-H. Yu, *Angew. Chem. Int. Ed.*, 2012, **51**, 7420-7425.
31. Z. P. Liu, Z. K. Hu, Q. Xie, B. J. Yang, J. Wu and Y. T. Qian, *J. Mater. Chem.*, 2003, **13**, 159-162.
32. D.-B. Jeong, J.-H. Lim, J. Lee, H. Park, M. Zhang, Y.-I. Lee, Y.-H. Choa and N. V. Myung, *Electrochim. Acta*, 2013, **111**, 200-205.
33. M. S. Mo, J. H. Zeng, X. M. Liu, W. C. Yu, S. Y. Zhang and Y. T. Qian, *Adv. Mater.*, 2002, **14**, 1658-1662.
34. X. Wang, Y. Xu, H. Zhu, R. Liu, H. Wang and Q. Li, *CrystEngComm.*, 2011, **13**, 2955-2959.
35. G. D. Lilly, Y. Chen, X. Pan and N. A. Kotov, *J. Phys. Chem. C*, 2010, **114**, 2428-2433.
36. D. H. Webber and R. L. Brutchey, *Chem. Commun.*, 2009, 5701-5703.
37. N. Watanabe and N. Toshima, *Bull. Chem. Soc. Jpn.*, 2007, **80**, 208-214.
38. U. K. Gautam, G. Gundiah and G. U. Kulkarni, *Solid State Commun.*, 2005, **136**, 169-172.
39. R. Haakenaasen, E. Selvig, S. Foss, L. Trosdahl-Iversen and J. Tafto, *Appl. Phys. Lett.*, 2008, **92**, 133108.
40. Y. Cheng, X. D. Han, X. Q. Liu, K. Zheng, Z. Zhang, T. Zhang, Z. T. Song, B. Liu and S. L. Feng, *Appl. Phys. Lett.*, 2008, **93**, 183113.
41. B. Kim and B.-K. Park, *Electron. Mater. Lett.*, 2012, **8**, 33-36.
42. R. B. Zheng, W. L. Cheng, E. K. Wang and S. J. Dong, *Chem. Phys. Lett.*, 2004, **395**, 302-305.
43. W. Zhu, W. Wang, H. Xu, L. Zhou, L. Zhang and J. Shi, *J. Cryst. Growth*, 2006, **295**, 69-74.